

Halo Abundance and Assembly History with Extreme-Axion Wave Dark Matter at $z \geq 4$

Hsi-Yu Schive,^{1*} Tzihong Chiueh^{2,3,4}

¹*National Center for Supercomputing Applications, Urbana, IL, 61801, USA*

²*Department of Physics, National Taiwan University, 10617 Taipei, Taiwan*

³*Institute of Astrophysics, National Taiwan University, 10617 Taipei, Taiwan*

⁴*Center for Theoretical Sciences, National Taiwan University, 10617 Taipei, Taiwan*

Accepted XXX. Received YYY; in original form ZZZ

ABSTRACT

Wave dark matter (ψ DM) composed of extremely light bosons ($m_\psi \sim 10^{-22}$ eV), with quantum pressure suppressing structures below a kpc-scale de Broglie wavelength, has become a viable dark matter candidate. Compared to the conventional free-particle ψ DM (FP ψ DM), the extreme-axion ψ DM model (EA ψ DM) proposed by Zhang & Chiueh (2017) features a larger cut-off wavenumber and a broad spectral bump in the matter transfer function. Here we conduct cosmological simulations to compare the halo abundances and assembly histories at $z = 4$ –11 between three different scenarios: FP ψ DM, EA ψ DM, and cold dark matter (CDM). We show that EA ψ DM produces significantly more abundant low-mass haloes than FP ψ DM with the same m_ψ , and therefore could alleviate the tension in m_ψ required by the Ly α forest data and by the kpc-scale dwarf galaxy cores. We also find that, compared to the CDM counterparts, massive EA ψ DM haloes are on average 3–4 times more massive at $z = 10$ –11 due to their earlier formation, undergo a slower mass accretion at $7 \lesssim z \lesssim 11$, and then show a rapidly rising major merger rate exceeding CDM by $\sim 50\%$ at $4 \lesssim z \lesssim 7$. This fact suggests that EA ψ DM haloes may exhibit more prominent starbursts at $z \lesssim 7$.

Key words: cosmology: dark matter – galaxies: high-redshift – galaxies: luminosity function, mass function – galaxies: evolution

1 INTRODUCTION

Wave dark matter (ψ DM, Hu et al. 2000; Schive et al. 2014a) has become a promising dark matter candidate. In this model, the dark matter is assumed to be composed of extremely light bosons with a mass of $m_\psi \sim 10^{-22}$ eV, where the uncertainty principle leads to a quantum pressure suppressing cosmic structures below the kpc scale. It thus provides a plausible solution to the small-scale issues found in the dissipationless cold dark matter (CDM) simulations (Weinberg et al. 2013). See Marsh (2016) and Hui et al. (2017) for comprehensive reviews on ψ DM.

The axion model is a ψ DM candidate, for which the field potential is specified by a cosine potential, $V(\theta) = m_\psi^2(1 - \cos(\theta))$, where θ is the axion angle. In the very early epoch of radiation era, the initial angle of the background field, $\theta_0 \equiv \pi - \delta\theta_0$, is frozen to $0 \leq \theta_0 \leq \pi$. After the Compton length of the particle enters the horizon, the background field starts to oscillate in the cosine potential.

This is a damped oscillation due to Hubble friction. Therefore, the angle rapidly sinks to the bottom of the potential ($\theta \ll 1$) and samples the harmonic oscillator potential, from which point on axions practically become free particles. The free-particle ψ DM (FP ψ DM) model in this context assumes $\theta_0 \ll 1$ and therefore the field executes simple harmonic oscillation right from the beginning (Zhang & Chiueh 2017a).

It turns out that perturbations of damped oscillations with different degrees of nonlinearity have little difference in their spectra evaluated at the radiation-matter equality, except for the extreme case where $\delta\theta_0 \ll 1$ (i.e., $\theta_0 \sim \pi$), the extreme-axion ψ DM (EA ψ DM) model (Zhang & Chiueh 2017b). Here the initial field is located near the unstable equilibrium on the potential top, and hence the oscillation can be substantially delayed compared with other initial angles. The delay weakens the role of Hubble friction and excites a parametric instability arising from small residual nonlinearity in the oscillation. This instability is weak but gets stronger when $\delta\theta_0 \rightarrow 0$. In this paper we take $\delta\theta_0 = 0.2^\circ$ as a representative example.

Generally speaking, there are two categories of con-

* E-mail: hyschive@ncsa.illinois.edu

straints on the ψ DM particle mass, $m_{22} \equiv m_\psi/10^{-22}$ eV. The first class of constraints addresses the kpc-scale cores found in the dwarf spheroidal galaxies, leading to $m_{22} \sim 1$ (e.g., Schive et al. 2014a; Chen et al. 2017) since the larger the particle mass, the smaller the core. The second class of constraints focuses on the abundance and size of cosmic small-scale structures, especially at higher redshifts. For example, the Ly α forest data suggest $m_{22} \gtrsim 10$ (Iršič et al. 2017; Armengaud et al. 2017), and the high- z luminosity functions and reionization imply $m_{22} \gtrsim 1$ (e.g., Schive et al. 2016; Corasaniti et al. 2017). There is thus a moderate but distinct tension between the two types of constraints, which is similar to, but not as severe as, the “Catch 22” problem of warm dark matter (Macciò et al. 2012). As found by Zhang & Chiueh (2017a,b), EA ψ DM predicts significantly more abundant small-scale structures and therefore low-mass haloes compared to FP ψ DM with the same particle mass, and thus could alleviate this tension. Here we report the first quantitative study on this subject.

This paper is structured as follows. We describe the simulation setup in Section 2 and show the results of halo mass function and assembly history in Section 3. Finally, we discuss and summarize our findings in Section 4.

2 SIMULATIONS

2.1 Initial Power Spectra

In the ψ DM scenario, quantum pressure resulting from the uncertainty principle suppresses the small-scale structures below a characteristic Jeans scale. This suppression can be expressed by the CDM-to- ψ DM transfer function, $T_{\psi\text{DM}}^2(k, z) = P_{\psi\text{DM}}(k, z)/P_{\text{CDM}}(k, z)$, where P is the power spectrum. Although $T_{\psi\text{DM}}(k, z)$ is in general redshift-dependent, Schive et al. (2016) showed that it can be well approximated as redshift-independent for the particle masses ($m_{22} \sim 1$), redshifts ($z \sim 4$ –11), and halo masses ($M_h \gtrsim 10^9 M_\odot$) relevant to this work, mainly because the Jeans mass is well below $10^9 M_\odot$.

The FP ψ DM transfer function is given by (Hu et al. 2000)

$$T_{\text{FP}\psi\text{DM}}(x) \approx \frac{\cos x^3}{1 + x^8}, \quad x = 1.61 m_{22}^{1/18} \frac{k}{k_{J,\text{eq}}}, \quad (1)$$

where $k_{J,\text{eq}} = 9 m_{22}^{1/2} \text{Mpc}^{-1}$ is the Jeans wavenumber at the matter-radiation equality. It exhibits a sharp cut-off at $k \sim k_{J,\text{eq}}$ and strong oscillations for $k > k_{J,\text{eq}}$. In comparison, the EA ψ DM transfer function with the same particle mass features a larger cut-off wavenumber and a spectral bump before the cut-off (see Fig. 3 in Zhang & Chiueh 2017b).

Fig. 1 compares the linear matter power spectra of CDM, FP ψ DM, and EA ψ DM at $z = 100$. We adopt the fiducial cosmological parameters of $\Omega_m = 0.30$, $\Omega_\Lambda = 0.70$, $\Omega_b = 0.06$, $h = 0.70$, and ψ DM parameters of $m_{22} = 1.1$ and $\delta\theta_0 = 0.2^\circ$. The EA ψ DM power spectrum shows a broad spectral bump peaking at $k \sim 8 h \text{Mpc}^{-1}$ and exceeding the CDM power spectrum by a factor of five, suggesting a significant excess of haloes with $M_h \sim 3 \times 10^{10} M_\odot$. In addition, the EA ψ DM power spectrum exhibits a cut-off wavenumber about a factor of two larger than that of FP ψ DM, indicative of significantly more haloes below $\sim 10^{10} M_\odot$. We quantify these differences from cosmological simulations in Section 3.

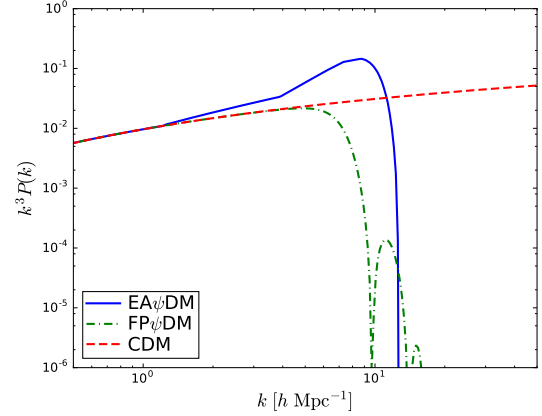


Figure 1. Linear power spectra of CDM, FP ψ DM, and EA ψ DM at $z = 100$. Both ψ DM power spectra feature a strong suppression at the high- k end, while EA ψ DM shows a broad spectral bump peaking at $k \sim 8 h \text{Mpc}^{-1}$ and a cut-off wavenumber roughly twice larger than that of FP ψ DM.

2.2 Simulation Setup

Genuine ψ DM simulations solving the Schrödinger-Poisson equation are extremely time-consuming since the matter wave dispersion relation demands exceptionally high spatial and temporal resolutions to resolve the wave function accurately (e.g., Schive et al. 2014a,b). However, Schive et al. (2016) shows that collisionless N -body simulations with ψ DM initial power spectra can be adopted to study the ψ DM evolution as long as the dynamical effect of quantum pressure is negligible for the redshifts and halo masses of interest. In this work, we focus on haloes more massive than $\sim 2 \times 10^9 M_\odot$, an order of magnitude higher than the ψ DM Jeans mass with $m_{22} \sim 1$ at $z \sim 10$, and we do not address the internal structure of haloes (e.g., the cuspy or cored density profiles). Therefore, it is sufficient for our purpose to conduct the collisionless N -body simulations.

We use the CAMB package (Lewis et al. 2000) for generating the CDM transfer function, the MUSIC code (Hahn & Abel 2011) for constructing the initial conditions, and the GADGET-2 code (Springel 2005) for the N -body simulations. We adopt a fiducial simulation configuration of $(L, N) = (80 h^{-1} \text{Mpc}, 1024^3)$, where L^3 is the comoving box size and N is the total number of simulation particles. It corresponds to a particle mass resolution of $\sim 5.7 \times 10^7 M_\odot$. This configuration is chosen to both accommodate a sufficient number of haloes above $\sim 10^{12} M_\odot$ at $z \sim 4$ and to capture the decline of ψ DM halo mass function below $\sim 10^{10} M_\odot$. We also conduct simulations with $(L, N) = (50 h^{-1} \text{Mpc}, 1024^3)$ and $(160 h^{-1} \text{Mpc}, 1024^3)$ to validate the numerical convergence. For each configuration, we conduct CDM, FP ψ DM, and EA ψ DM simulations from $z = 100$ to 4.

3 RESULTS

Fig. 2 shows the projected dark matter density centered on one of the most massive haloes in the simulations at $z = 4$ –10, which is unambiguously identified in all three models. At $z = 10$, the EA ψ DM halo has a mass of $M_h \sim 2.3 \times 10^{11} M_\odot$, about two and three times more massive than

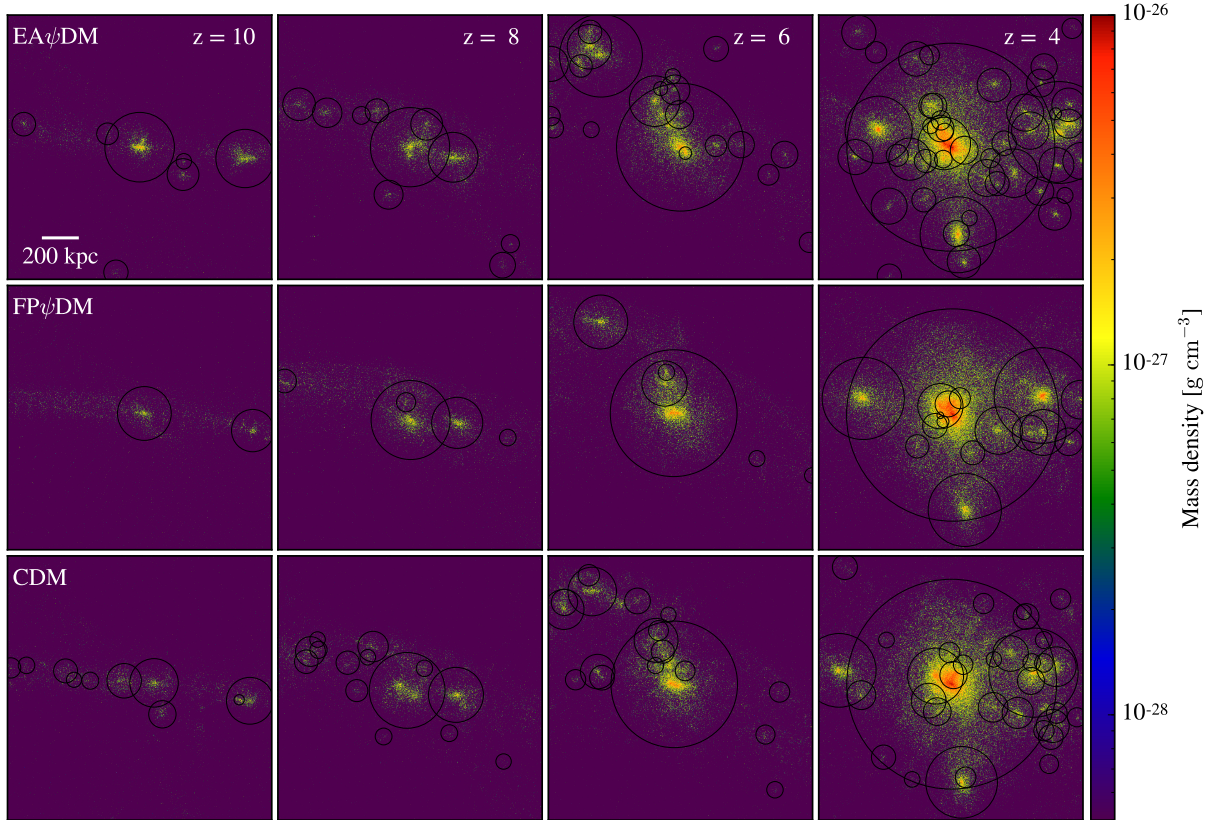


Figure 2. Projected dark matter density in a $1\ h^{-1}\text{Mpc}$ thick slab centered on a representative massive halo in the simulations. Different rows represent different dark matter models, and different columns represent different redshifts. Circles depict the halo virial radii. This halo has a similar mass of $M_h \sim 6.5 \times 10^{12} M_\odot$ at $z = 4$ in all three models but is apparently more massive in EA ψ DM at $z = 10$. In addition, FP ψ DM shows significantly fewer low-mass haloes at all redshifts. These facts suggest very different halo formation histories in different models. See text for details. The images are produced with the analysis toolkit yt (Turk et al. 2011).

the FP ψ DM and CDM counterparts, respectively. However, at $z = 4$, the halo masses in different models converge to $M_h \sim (6.3\text{--}6.7) \times 10^{12} M_\odot$. Furthermore, FP ψ DM shows significantly fewer low-mass haloes at all redshifts. These facts suggest very different halo mass functions and assembly histories in different models, particularly at higher redshifts. We provide quantitative analyses in this section.

3.1 Halo Mass Function

Fig. 3 shows the halo mass function (MF) at $z = 4\text{--}10$ and the MF ratios between different models. We use the AMIGA Halo Finder (Knollmann & Knebe 2009) to identify all haloes with at least 40 particles, corresponding to a minimum halo mass of $\sim 2.3 \times 10^9 M_\odot$ in a $L = 80\ h^{-1}\text{Mpc}$ box. To validate the results, we compare the simulated CDM MF to the analytical prediction of Sheth & Tormen (1999) and demonstrate a good agreement, especially at lower redshifts. We also verify that the MFs shown in Fig. 3, particularly at the low- and high-mass ends, are consistent with simulations with $L = 50\ h^{-1}\text{Mpc}$ and $160\ h^{-1}\text{Mpc}$.

The EA ψ DM MF is found to outnumber CDM in a wide mass range from several times $10^9 M_\odot$ to several times $10^{11} M_\odot$, with the maximum difference at $\sim 3 \times 10^{10} M_\odot$. It is consistent with the EA ψ DM power spectrum with a broad spectral bump peaking at $k \sim 8\ h\text{Mpc}^{-1}$ (see Fig. 1).

The excess of the EA ψ DM MF is more prominent at higher redshifts, reaching a factor of $\sim 10\text{--}30$ higher than CDM for $M_h \sim 10^{10}\text{--}10^{11} M_\odot$ at $z = 10$. By contrast to the CDM haloes with similar masses, these abundant high- z EA ψ DM haloes are the first collapsed objects which accrete mass mainly by smooth mass accretion due to the strong suppression of low-mass haloes and form earlier because of the higher local overdensity.

The difference between the EA ψ DM and CDM MFs above $\sim 10^{10} M_\odot$ diminishes at lower redshifts but is still about two- to threefold for $M_h \sim 10^{10}\text{--}10^{11} M_\odot$ at $z = 4$. Moreover, EA ψ DM has substantially more haloes than FP ψ DM even below $\sim 10^{10} M_\odot$, although both simulations adopt $m_{22} = 1.1$. These unique features in EA ψ DM may have a distinct impact on constraining m_{22} , which we will discuss in Section 4.

In comparison, the FP ψ DM MF never exceeds CDM and drops significantly for $M_h \lesssim 3 \times 10^{10} M_\odot$. Moreover, unlike EA ψ DM, the ratio between the FP ψ DM and CDM MFs is found to be almost redshift-independent, in agreement with the previous study (Schive et al. 2016).

Particle simulations with an initial power spectrum cut-off are known to suffer from the formation of low-mass spurious haloes, mostly confined along cosmic filaments and resulting in an unphysical upturn at the low-mass end of MF (e.g., Wang & White 2007). However, we do not detect either

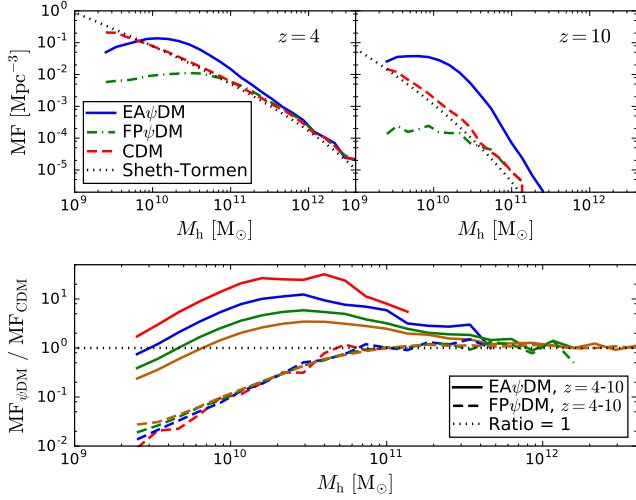


Figure 3. Halo mass functions (MF) in logarithmic mass bins. The upper panels show the MFs at $z = 4$ and 10 , where the dotted lines represent the analytical prediction of [Sheth & Tormen \(1999\)](#) for CDM. The lower panel shows the MF ratios between ψ DM and CDM at $z = 10$ (red), 8 (blue), 6 (green), and 4 (brown). EA ψ DM MF outnumbers CDM in a wide mass range from several times $10^9 M_\odot$ to several times $10^{11} M_\odot$, especially at higher redshifts. In comparison, FP ψ DM has significantly fewer low-mass haloes. See text for details.

of these artificial features, suggesting that the contamination from spurious haloes is minimal. It is likely because the spurious haloes are more prominent for $M_h \lesssim 10^9 M_\odot$ with $m_{22} \sim 1$ ([Schive et al. 2016](#)), which is beyond the minimum halo mass adopted here.

3.2 Halo Assembly History

Figs 2 – 3 suggest very different assembly histories between massive ψ DM and CDM haloes, which we detail below. We select all haloes more massive than $10^{12} M_\odot$ at $z = 4$, leading to ~ 170 candidates in each model, and trace their progenitors to $z = 11$. We define major mergers as those with progenitor mass ratio above $1 : 3$.

Fig. 4 shows various aspects of the halo assembly history. The upper left panel shows the mean major merger rate per halo per unit z . The most striking feature in EA ψ DM is the apparently higher major merger rate at $4 \lesssim z \lesssim 7$, exceeding CDM by $\sim 50\%$, followed by a sharp transition at $z \sim 7$. This feature is verified to be insensitive to the adopted progenitor mass ratio. In comparison, FP ψ DM exhibits a much lower merger rate at higher redshifts due to the strong suppression of low-mass haloes. The upper right panel shows the fraction of mass accretion rate via major mergers. This ratio is found to be less than $\sim 30\%$ in all cases, suggesting that major mergers do not dominate mass accretion even for EA ψ DM.

The lower left panel shows the mean mass assembly history, defined as the halo mass ratio between $z > 4$ and $z = 4$. Importantly, the EA ψ DM curve is found to be significantly higher at $z \gtrsim 7$, reaching a factor of 3–4 higher than CDM at $z = 10$ – 11 , while all curves converge at $z \lesssim 7$. Since all models have similar halo MFs for $M_h \gtrsim 10^{12} M_\odot$ at $z = 4$ (see

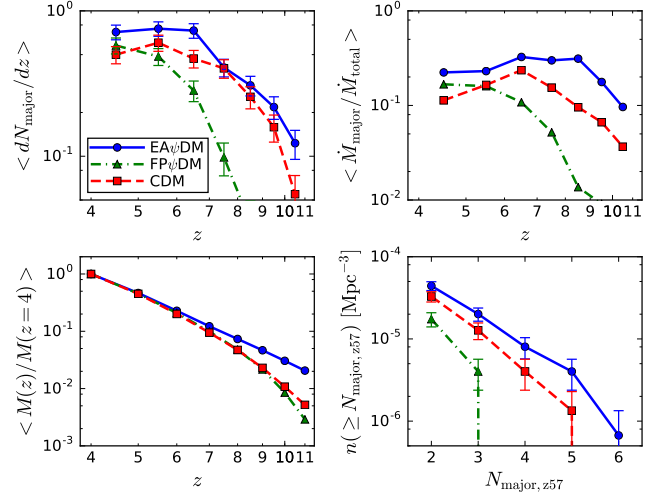


Figure 4. Halo assembly history at $4 \leq z \leq 11$: the mean major merger rate per halo per unit z (upper left), the fraction of mass accretion rate via major merger (upper right), the mean mass assembly history (lower left), and the cumulative halo number density with at least $N_{\text{major},z57}$ major mergers at $5 \leq z < 7$ and at most one major merger at $4 \leq z < 5$ (lower right). Error bars are Poisson counting uncertainties. See text for details.

Fig. 3), the mean mass assembly fraction shown here can be regarded as approximately proportional to the average halo mass. Therefore, it shows that compared to the CDM counterparts, massive EA ψ DM haloes (i) form at higher redshifts, (ii) are a factor or 3–4 more massive at $z = 10$ – 11 , and (iii) experience a slower mass accretion at $7 \lesssim z \lesssim 11$.

In EA ψ DM, the findings of a smooth mass accretion at $7 \lesssim z \lesssim 11$ followed by a steeply rising major merger rate at $z \sim 7$ indicate that a substantial halo population may experience a rapidly increasing star formation at $z \lesssim 7$. Interestingly, recent observations show that $\sim 35\%$ of massive galaxies at $z \sim 4$ are quiescent, with a stellar masses of $\sim 10^{11} M_\odot$, a number density of $(1.8 \pm 0.7) \times 10^{-5} \text{ Mpc}^{-3}$, and an exceedingly efficient star formation at $5 \lesssim z \lesssim 7$ ([Straatman et al. 2014](#); [Glazebrook et al. 2017](#)), although still under debate ([Simpson et al. 2017](#)). These features cannot be easily explained by current CDM simulations (e.g., [Rodriguez-Gomez et al. 2016](#)). To investigate this issue in the context of EA ψ DM, we show in the lower right panel of Fig. 4 the cumulative halo number density with *at least* $N_{\text{major},z57}$ major mergers at $5 \leq z < 7$ and *at most* one major merger at $4 \leq z < 5$. Intriguingly, we find that EA ψ DM haloes have a noticeably higher number density of these extreme events, exceeding CDM by factors of 2 and 3 for $N_{\text{major},z57} \geq 4$ and 5, respectively, and reaching $(8.1 \pm 2.3) \times 10^{-6} \text{ Mpc}^{-3}$ for $N_{\text{major},z57} \geq 4$. It suggests that compared to CDM, massive EA ψ DM haloes may exhibit more prominent starbursts at $5 \lesssim z \lesssim 7$.

Note, however, that the CDM simulations of [Rodriguez-Gomez et al. \(2016\)](#) have a box size of as large as $\sim 100^3 \text{ Mpc}^3$, implying that EA ψ DM may not completely solve the puzzle since it only increases the number of candidates by a factor of 2–3. Moreover, $\sim 75\%$ of EA ψ DM haloes with $N_{\text{major},z57} \geq 4$ shown in Fig. 4 still undergo one major merger at $4 \leq z < 5$ and thus may not be fully qui-

escent. Larger hydrodynamical simulations, ideally coupled with dynamical quantum effect, are necessary for addressing this subject in more detail.

4 DISCUSSION AND SUMMARY

In this paper, we have conducted cosmological simulations to compare the halo mass functions (MF) and assembly histories between three different dark matter models, namely, the extreme-axion wave dark matter (EA ψ DM, Zhang & Chiueh 2017b), the free-particle wave dark matter (FP ψ DM, Hu et al. 2000; Schive et al. 2014a), and the cold dark matter (CDM). Both ψ DM models feature a strong suppression of low-mass haloes, the scale of which is mainly determined by the dark matter particle mass (m_{22}). However, the EA ψ DM model introduces a second free parameter, the initial field angle $\delta\theta_0$, which, for the same m_{22} , can result in a dark matter transfer function with a larger cut-off wavenumber and a broad spectral bump before the cut-off (see Fig. 1). Both features are expected to produce more abundant low-mass haloes and significantly alter the halo formation history. The main motivation of this work is to quantify these effects.

Our major results can be summarized as follows.

- EA ψ DM MF outnumber CDM in a wide mass range peaking at $M_h \sim 3 \times 10^{10} M_\odot$. The MF excess is more prominent at higher redshifts, reaching a factor of 2–3 at $z \sim 4$ and exceeding an order of magnitude at $z \sim 10$ (see Fig. 3).
- EA ψ DM MF at $M_h \lesssim 3 \times 10^{10}$ is in excess of FP ψ DM by one and two orders of magnitude at $z \sim 4$ and $z \sim 10$, respectively (see Fig. 3).
- Compared to the CDM counterparts, massive EA ψ DM haloes are on average 3–4 times more massive at $z = 10$ –11 due to their earlier formation, and then undergo a slower mass accretion at $z \gtrsim 7$. Afterward, their mean major merger rate rises sharply and exceeds CDM by $\sim 50\%$ at $4 \lesssim z \lesssim 7$ (see the upper and lower left panels of Fig. 4), suggesting more prominent starbursts in EA ψ DM haloes at this epoch.

The finding of substantially more low-mass haloes in EA ψ DM compared to FP ψ DM with the same m_{22} may have a distinct impact on constraining m_{22} . If we naively estimate an effective particle mass $m_{22,\text{eff}}$ of EA ψ DM by equating the cumulative halo MFs, $n_{\text{EA}\psi\text{DM}}(\geq M_{\min}, m_{22}) = n_{\text{FP}\psi\text{DM}}(\geq M_{\min}, m_{22,\text{eff}})$, with $m_{22} \sim 1$ and an arbitrarily small M_{\min} (e.g., $\sim 10^8 M_\odot$), we obtain $m_{22,\text{eff}} \sim 5m_{22}$ at $z = 4$. Since the core radii of ψ DM haloes are determined by m_{22} instead of $m_{22,\text{eff}}$, it thus suggests that EA ψ DM could reduce the tension in m_{22} required by the Ly α forest ($m_{22} \gtrsim 10$, Iršič et al. 2017; Armengaud et al. 2017), the high- z luminosity functions and reionization ($m_{22} \gtrsim 1$, e.g., Schive et al. 2016; Corasaniti et al. 2017), and the kpc-scale cores of dwarf spheroidal galaxies ($m_{22} \sim 1$, e.g., Schive et al. 2014a; Chen et al. 2017). Moreover, note that this definition of $m_{22,\text{eff}}$ only considers the halo number density and disregards the fact that EA ψ DM haloes are on average more massive, and thus we should regard it as a conservative lower limit in this sense. Also, the choice of $\delta\theta_0 = 0.2^\circ$ in this work is to some degree arbitrary to demonstrate the effect of the EA ψ DM model, and a somewhat smaller $\delta\theta_0$ may alleviate this tension further. Regardless of this possibility,

ψ DM simulations coupled with both dynamical quantum effect and baryons are essential for a more quantitative study on this subject.

5 ACKNOWLEDGEMENT

We thank Ui-Han Zhang for providing the initial EA ψ DM power spectrum. The simulations were conducted on the Campus Cluster at the University of Illinois at Urbana-Champaign. This work is supported in part by MOST of Taiwan under the grant MOST 103-2112-M-002-020-MY3.

REFERENCES

- Armengaud E., Palanque-Delabrouille N., Yèche C., Marsh D. J. E., Baur J., 2017, preprint, ([arXiv:1703.09126](#))
- Chen S.-R., Schive H.-Y., Chiueh T., 2017, *MNRAS*, **468**, 1338
- Corasaniti P. S., Agarwal S., Marsh D. J. E., Das S., 2017, *Phys. Rev. D*, **95**, 083512
- Glazebrook K., et al., 2017, *Nature*, **544**, 71
- Hahn O., Abel T., 2011, *MNRAS*, **415**, 2101
- Hu W., Barkana R., Gruzinov A., 2000, *Physical Review Letters*, **85**, 1158
- Hui L., Ostriker J. P., Tremaine S., Witten E., 2017, *Phys. Rev. D*, **95**, 043541
- Iršič V., Viel M., Haehnelt M. G., Bolton J. S., Becker G. D., 2017, preprint, ([arXiv:1703.04683](#))
- Knollmann S. R., Knebe A., 2009, *ApJS*, **182**, 608
- Lewis A., Challinor A., Lasenby A., 2000, *ApJ*, **538**, 473
- Macciò A. V., Paduroiu S., Anderhalden D., Schneider A., Moore B., 2012, *MNRAS*, **424**, 1105
- Marsh D. J. E., 2016, *Phys. Rep.*, **643**, 1
- Rodriguez-Gomez V., et al., 2016, *MNRAS*, **458**, 2371
- Schive H.-Y., Chiueh T., Broadhurst T., 2014a, *Nature Physics*, **10**, 496
- Schive H.-Y., Liao M.-H., Woo T.-P., Wong S.-K., Chiueh T., Broadhurst T., Hwang W.-Y. P., 2014b, *Physical Review Letters*, **113**, 261302
- Schive H.-Y., Chiueh T., Broadhurst T., Huang K.-W., 2016, *ApJ*, **818**, 89
- Sheth R. K., Tormen G., 1999, *MNRAS*, **308**, 119
- Simpson J. M., et al., 2017, preprint, ([arXiv:1704.03868](#))
- Springel V., 2005, *MNRAS*, **364**, 1105
- Straatman C. M. S., et al., 2014, *ApJ*, **783**, L14
- Turk M. J., Smith B. D., Oishi J. S., Skory S., Skillman S. W., Abel T., Norman M. L., 2011, *ApJS*, **192**, 9
- Wang J., White S. D. M., 2007, *MNRAS*, **380**, 93
- Weinberg D. H., Bullock J. S., Governato F., Kuzio de Naray R., Peter A. H. G., 2013, preprint ([arXiv:1306.0913](#))
- Zhang U.-H., Chiueh T., 2017b, preprint, ([arXiv:1705.01439](#))
- Zhang U.-H., Chiueh T., 2017a, preprint, ([arXiv:1702.07065](#))

This paper has been typeset from a T_EX/L^AT_EX file prepared by the author.